

# Evaluating Feature Attribution: An Information-Theoretic Perspective

Yao Rong<sup>\*1</sup> Tobias Leemann<sup>\*1</sup> Vadim Borisov<sup>1</sup> Gjergji Kasneci<sup>1,2</sup> Enkelejda Kasneci<sup>1</sup>

## Abstract

With a variety of local feature attribution methods being proposed in recent years, follow-up work suggested several evaluation strategies. To assess the attribution quality across different attribution techniques, the most popular among these evaluation strategies in the image domain use pixel perturbations. However, recent advances discovered that different evaluation strategies produce conflicting rankings of attribution methods and can be prohibitively expensive to compute. In this work, we present an information-theoretic analysis of evaluation strategies based on pixel perturbations. Our findings reveal that the results output by different evaluation strategies are strongly affected by information leakage through the shape of the removed pixels as opposed to their actual values. Using our theoretical insights, we propose a novel evaluation framework termed Remove and Debias (ROAD) which offers two contributions: First, it mitigates the impact of the confounders, which entails higher consistency among evaluation strategies. Second, ROAD does not require the computationally expensive retraining step and saves up to 99% in computational costs compared to the state-of-the-art. Our source code is available at [https://github.com/tleemann/road\\_evaluation](https://github.com/tleemann/road_evaluation).

## 1. Introduction

Explainable Artificial Intelligence (XAI) is a widely discussed research topic (Adadi & Berrada, 2018). Specifically, feature attribution methods (Springenberg et al., 2015; Ribeiro et al., 2016; Lundberg & Lee, 2017; Sundararajan et al., 2017; Selvaraju et al., 2017) that quantify the importance of input features to a model’s

<sup>\*</sup>Equal contribution <sup>1</sup>Department of Computer Science, University of Tübingen, Tübingen, Germany <sup>2</sup>SCHUFA Holding AG, Wiesbaden, Germany. Correspondence to: Yao Rong <yao.rong@uni-tuebingen.de>, Tobias Leemann <tobias.leemann@uni-tuebingen.de>.

Preliminary work.

Rank	1	2	3	
MoRF	IG	IG-Var	IG-SG	<b>Removal evaluation strategy (e.g., ROAR)</b> • Consistency: <b>Low</b> • Computation : <b>100 min</b>
LeRF	IG-SG	IG	IG-Var	
↓ debiasing				
Rank	1	2	3	
MoRF	IG-SG	IG	IG-Var	<b>Debaised removal evaluation strategy</b> • Consistency: <b>High</b> • Computation : <b>100 min</b>
LeRF	IG-SG	IG	IG-Var	
↓ agrees with				
Rank	1	2	3	
MoRF	IG-SG	IG	IG-Var	<b>ROAD (ours)</b> • No retraining • Consistency: <b>High</b> • Computation : <b>43 sec</b>
LeRF	IG-SG	IG	IG-Var	

Figure 1. Comparison between previous removal and retraining evaluation strategies (**Top**) and ours (**Bottom**). Previously, rankings of different attribution methods, Integrated Gradients (IG) (Sundararajan et al., 2017) and its two variants SmoothGrad (IG-SG) (Smilkov et al., 2017), SmoothGrad<sup>2</sup> (IG-SQ) (Hooker et al., 2019), are highly inconsistent with respect to hyperparameters such as the removal orders Most Relevant First (MoRF) and Least Relevant First (LeRF). Our ROAD strategy achieves a consistent ranking using only 1% of the previously required resources.

decision are widely used. Such local explanations can help to analyze and debug predictive models (Bhatt et al., 2020b; Adebayo et al., 2020), e.g., in the medical domain (Eitel et al., 2019), recommender systems (Afchar & Hennequin, 2020), and many other applications. With an increasing number of feature attribution methods proposed in the literature, the need for sound strategies to evaluate these methods is also increasing (Nguyen & Martínez, 2020; Hase & Bansal, 2020; Yeh et al., 2019; Hooker et al., 2019).

Unfortunately, for real-world data sets, ground truth attributions are usually not available. Therefore, evaluation strategies, proposed to compare different attribution methods, commonly follow an ablation approach by perturbing the input features, e.g., image pixels, deemed most or least important. Specifically, perturbing pixels assigned high importance should decrease predictive quality whereas perturbing unimportant pixels, should hardly affect the predictions. These measures aim to capture the *fidelity* of explanations (Tomsett et al., 2020), i.e., how well the explanation genuinely reflects the prediction of the underlying model. Fidelity based on a single data sample is

known as local fidelity, while global fidelity is measured on the whole data set (Tomsett et al., 2020).

The outcome of evaluation strategies is highly sensitive to parameters such as the perturbation function and order. Depending on the order chosen, i.e., *most relevant pixels first* or *least relevant pixels first*, such removal strategies often lead to highly contradictory results. For instance, local attribution methods that seem to perform well in one order may perform rather poorly in the other (Tomsett et al., 2020; Haug et al., 2021; Hooker et al., 2019). This inconsistency makes it hard for researchers to impartially compare between different attribution methods and it is not well understood where the inconsistencies stem from. Moreover, for conducting the global fidelity check, a retraining step is required by some methods (Hooker et al., 2019), which is prohibitively expensive in practice (Tomsett et al., 2020). These two drawbacks and our improvements are illustrated in Figure 1.

In this paper, we aim to overcome these shortcomings and make the evaluation more consistent and efficient. To achieve this, we propose a new debiased strategy that compensates for confounders causing inconsistencies. Furthermore, we show that in the debiased setting, we can skip the retraining without significant changes in the results. This results in drastic efficiency gains as shown in the lower part of Figure 1. We argue that it is crucial for the community to have sound evaluation strategies that do not suffer from limited accessibility due to the required compute capacity. Specifically, we make the following contributions:

- We examine the mechanisms underlying the evaluation strategies based on perturbation by conducting a rigorous information-theoretic analysis, and formally reveal that results can be significantly confounded.
- To compensate for this confounder, we propose the Noisy Linear Imputation strategy and empirically prove its efficiency and effectiveness. The proposed strategy significantly decreases the sensitivity to hyperparameters such as the removal order.
- We generalize our findings to a novel evaluation strategy, ROAD (RemOve And DeBias), which can be used to objectively and efficiently evaluate several attribution methods. Compared to previous evaluation strategies requiring retraining, e.g., Remove and Retrain (ROAR) (Hooker et al., 2019), ROAD saves 99% of the computational costs.

## 2. Related Work

There is a plethora of works on different explanation techniques (Tjoa & Guan, 2020), especially attribution methods that assign importance scores to each input features.

Popular approaches have been proposed by Springenberg et al. (2015); Bach et al. (2015); Ribeiro et al. (2016); Kasneci & Gottron (2016); Sundararajan et al. (2017); Fong & Vedaldi (2017); Shrikumar et al. (2017); Smilkov et al. (2017); Petsiuk et al. (2018); Adebayo et al. (2018); Chen et al. (2018); Xu et al. (2020), and many more scholars.

With the growing numbers of attribution methods, various scholars have presented desiderata that explanations, should fulfill (Bhatt et al., 2020a; Nguyen & Martínez, 2020; Fel et al., 2021; Afchar et al., 2021; Nauta et al., 2022). Doshi-Velez & Kim (2017) consider two subcategories in this field, namely *human-grounded* metrics relying on human judgement and *functional-grounded* metrics that do not require a human-generated ground truth. The latter frequently rely on the idea that if the most important part of the image is changed, the output probability of the given black-box model should also change in return. Examples include the Sensitivity-n measure proposed by Ancona et al. (2017) and the infidelity and max-sensitivity metrics by Yeh et al. (2019). Samek et al. (2016) and Petsiuk et al. (2018) also proposed to perturb the pixels in the input image according to the importance scores. However, Hooker et al. (2019) showed that the perturbation introduces artifacts and results in a distribution shift, putting these no-retraining approaches in question. They proposed the Remove and Retrain (ROAR) framework with an extensive model retraining step to adapt to the distribution shift. Therefore, we distinguish between evaluation methods with *retraining* and *no-retraining* approaches. ROAR has been adopted in several recent studies (Hartley et al., 2020; Izzo et al., 2020; Meng et al., 2021; Schramowski et al., 2020; Srinivas & Fleuret, 2019) and variations are being proposed in concurrent work (Shah et al., 2021).

Only few papers have used and compared different evaluation strategies for attribution methods and a sound theoretical explanation for the differences between them is still missing. Sturmfels et al. (2020) assess different baselines for feature attribution applying the Integrated Gradient (Sundararajan et al., 2017) method. They also observe that changing the hyperparameter settings can lead to varying results. Haug et al. (2021) draw the same conclusion for attributions on tabular data. Tomsett et al. (2020) compute the consistency among different, no-retraining evaluation strategies and report an alarmingly low agreement. In this work, we conduct a rigorous analysis of reasons for existing inconsistency and provide a solution to reduce it, which is not studied in previous works. Moreover, our solution also reduces high computational costs caused by retraining.

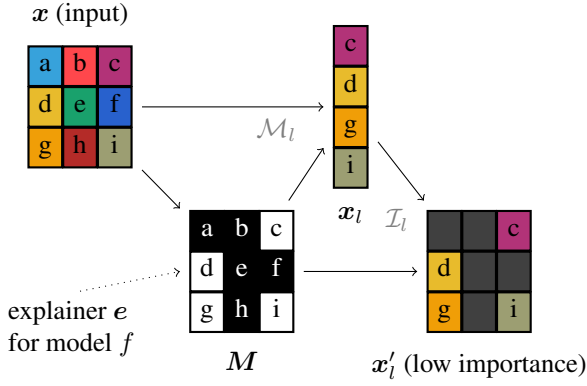


Figure 2. Our analytical model of feature removal evaluation (MoRF order shown): The input image  $x$  (9 pixels a–i) is explained by an explanation method that returns a mask  $M$  indicating important pixels (black). The remaining, less important pixel values  $x_l$  can be extracted from the image using the masking operator  $\mathcal{M}_l$  and transformed via the imputation operator  $\mathcal{I}_l$  to an imputed variant of the input  $x'_l$ , which determines the evaluation outcome. This model allows to separate the information in the feature values from that contained in the binary mask  $M$ .

### 3. Preliminaries

In this section, we formally define the pixel-perturbation strategies considered by the following analysis.

#### 3.1. Retraining Evaluation Strategies

We consider a pixel removal strategy, where pixels are successively replaced by imputed values. Consistent with the literature (Tomsett et al., 2020; Samek et al., 2016), we consider two removal orders: **MoRF** (Most Relevant First) or **LeRF** (Least Relevant First), where the subsequent removal starts with the most important pixels for the former and the least important ones for the latter. We now provide a formal definition of MoRF with retraining, i.e., the ROAR benchmark, that will be used throughout our analysis. We always use the MoRF order in the analysis presented in this paper. However, an analogous analysis of its counterpart LeRF is possible without much additional effort and can be found in the appendix.

To ease our derivations, we describe the procedure by a series of operations that can be analyzed independently. A classifier  $f : \mathbb{R}^d \rightarrow \{1, \dots, c\}$  maps inputs  $x \in \mathbb{R}^d$  to labels  $C \in \{1, \dots, c\}$ , where  $c$  is the number of classes. A feature attribution explanation for the prediction assigns each input dimension an importance value. In the MoRF setting, the features are ordered in a descending order of importance. Subsequently, the  $k$  most important features per instance are selected for removal, where  $0 \leq k \leq d$  is successively increased during the benchmark. However, for the moment we consider only one fixed value of  $k$ . Thus,

$C$	Class label random variable
$I$	Mutual information
$\mathcal{I}$	Imputation operator
$M$	Binary mask in $\{0, 1\}^d$
$\mathcal{M}$	Mask selection operator (takes out relevant features)
$x$	Input features in $\mathbb{R}^d$
$x_l$	Low importance features only in $\mathbb{R}^{k-d}$
$x'_l$	Imputed low importance features in $\mathbb{R}^d$

Table 1. Overview of the notation used in this work.

we can model the explanation  $e_k$  as a choice of features via a binary mask  $M = e_k(f, x) \in \{0, 1\}^d$ , with the corresponding value set to one, if the corresponding feature is among the top- $k$ , and to zero otherwise. Furthermore, suppose  $\mathcal{M}_l : \{0, 1\}^d \times \mathbb{R}^d \rightarrow \mathbb{R}^{d-k}$  to be the selection operator for the least important dimensions indicated in the mask and  $x_l = \mathcal{M}_l(M, x)$  to be a vector containing only the remaining features as shown in Figure 2. We suppose that the features preserve their internal order in  $x_l$ , i.e., features are ordered ascendingly by their original input indices. This definition allows to separately consider the information flow in the feature mask  $M$  and that in the feature values  $x_l$ .

The ROAR approach measures the accuracy of a newly trained classifier  $f'$  on modified samples  $x'_l := \mathcal{I}_l(M, x_l)$ , where  $\mathcal{I}_l : \{0, 1\}^d \times \mathbb{R}^{d-k} \rightarrow \mathbb{R}^d$  is an imputation operator that redistributes all inputs in the vector  $x_l$  to their original positions and sets the remainder to some filling value. In the special case of zero imputation,  $x'_l = \mathcal{I}_l(M, \mathcal{M}_l(M, x)) = (1 - M) \odot x$ . This means the top- $k$  features are discarded. For a better evaluation result, the accuracy should drop quickly with increasing  $k$ , indicating the most influential features were successfully removed.

#### 3.2. Information Theory

We now briefly revisit the central concepts of information theory that will be handy for our analysis and introduce the notation. The fundamental quantity in information theory is the entropy  $H$  of a discrete random variable  $X$  with support  $\text{supp}\{X\}$ ,

$$H(X) := - \sum_{x \in \text{supp}\{X\}} P(X = x) \log P(X = x). \quad (1)$$

The entropy corresponds to the information gained through observation of a realization of this variable. If the random variable considered can be easily inferred, we use  $p(x)$  as a shorthand for  $P(X = x)$ . Furthermore, we denote the joint entropy between random variables  $X$  and  $Y$  by  $H(X, Y)$ , which is equivalent to the entropy of their joint distribution. In accordance with (Cover & Thomas, 2006), we always separate random variables by comma to denote the joint

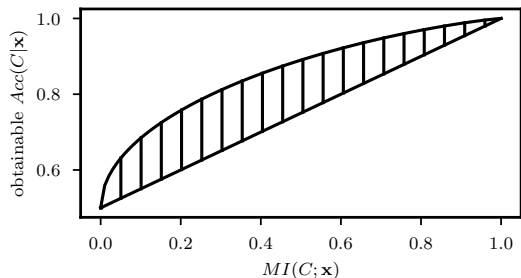


Figure 3. Relation between Mutual Information (MI) and obtainable accuracy for the two-class problem with equal class priors. The knowledge of the MI  $I(\mathbf{x}; C)$  implies strong bounds for the obtainable accuracy. This connection permits to use MI as a surrogate for the obtainable accuracy in the perturbation strategy in our analysis. Figure adapted from (Meyen, 2016).

distribution of multiple of variables.

The conditional entropy  $H(X|Y)$  is the expected amount of information left in a variable, given the observation of a condition  $Y$ . The most central concept in our analysis will be mutual information (MI), i.e., the amount of information in one random variable shared with another. For example, by  $I(\mathbf{x}; C) := H(C) - H(C|\mathbf{x})$ , we denote the MI between the complete feature vector and the class variable  $C$ . We separate arguments by a semicolon and allow single random variables or sets of random variables as arguments to all the defined quantities. For sets, we always consider the joint distribution of their member variables. Please confer (Cover & Thomas, 2006) for a more profound introduction. We provide a short overview of our notation in Table 1.

## 4. Analysis

In this section, we show that the pixel perturbation strategies are susceptible to a previously unknown confounder: The binary mask itself can leak class information that might not be present in the feature values. After making the connection between the accuracy and mutual information as a theoretical tool in Section 4.1, we formally derive the confounder and identify this leakage on real data in Section 4.2. We subsequently show how to mitigate it through Minimally Revealing Imputation in Section 4.3.

### 4.1. On the Relation Between Accuracy and Mutual Information

To begin our analysis of the presented strategies and their underlying mechanisms, we first establish the relation between classification accuracy and the mutual information. It is well-known that the classification performance of an optimal classifier in the Bayesian sense (assigning the class with the highest posterior) is dependent on the MI between features and labels (Hellman & Raviv, 1970; Vergara & Estévez, 2014; Meyen, 2016). Nevertheless, the relationship

is not a function, but comes in form of upper and lower bounds of the obtainable accuracy. For the simple two-class problem, the bounds are shown in Figure 3 (cf. Appendix A.1 for derivations). They impose strong limits on the optimal classification performance, if the mutual information  $I(\mathbf{x}; C)$  is known.

For the pixel removal strategies that use retraining, this allows us to analyze the frameworks using MI as a surrogate for the attainable accuracy because higher MI almost always leads to higher accuracy. In the MoRF setting with retraining,  $I(\mathbf{x}'_i; C)$  will play a key role, because it quantifies the information left in the least important features and thus determines obtainable accuracy which is the outcome of the evaluation. Low mutual information  $I(\mathbf{x}'_i; C)$  results in a sharp drop in accuracy and good benchmarking results:

$$\downarrow I(\mathbf{x}'_i; C) \Rightarrow \uparrow \text{MoRF benchmark}$$

Therefore, in the MoRF setting low mutual information of  $\mathbf{x}'_i$  and  $C$  is desirable.

### 4.2. Class Information Leakage through Masking

We demonstrate that it is easily possible to leak class information only through the mask’s shape and to harshly manipulate the evaluation score. Therefore, we start by separating the influence of the mask from that of the feature values. We apply the following identity:

$$\underbrace{I(\mathbf{x}'_i; C)}_{\text{Eval. Outcome}} = \underbrace{I(C; \mathbf{x}'_i | M)}_{\text{Feature Info.}} + \underbrace{I(C; M)}_{\text{Mask Info.}} - \underbrace{I(C; M | \mathbf{x}'_i)}_{\text{Mitigator}}. \quad (2)$$

The quantities involved are visualized in Figure 4a. The first term “Feature Information” is the class information contained in the features (and not in the mask) that we wish to estimate. The second term “Mask Information” shows that class discriminative information in the mask can have a high impact on the result. This influence can be compensated by the “Mitigator” term.

**Class Information Leakage** If the Mask Information term is superior to the Mitigator,  $I(C; M) > I(C; M | \mathbf{x}'_i)$ , the evaluation outcome is unfairly increased to a value not justified by the selected features. We term this phenomenon *Class Information Leakage*, as some discriminative information is “leaked” through the binary mask  $M$  used.

The Mitigator can entirely vanish when the mask is perfectly inferable from the imputed image  $\mathbf{x}'_i$ . This results in a non-compensated effect of Class Information Leakage. We define this imputation operation as follows:

**Condition 4.1.** *Invertible Imputation.* Let  $\mathcal{I}_l : \{0, 1\}^d \times \mathbb{R}^{d-k} \rightarrow \mathbb{R}^d$  be the imputation operator that takes the least

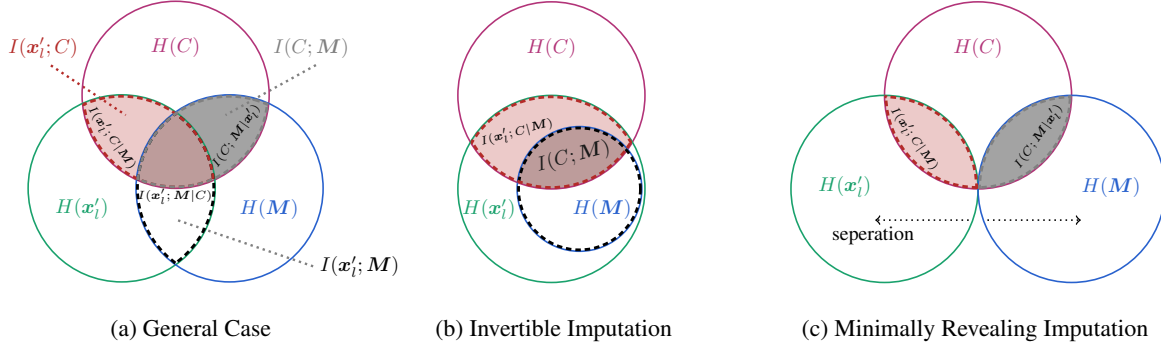


Figure 4. The Evaluation Outcome  $I(x'_i; C)$  (red area), is confounded by the Mask Information  $I(C; M)$  (gray area) when there is some overlap (a). Only the Feature Information  $I(x'_i; C|M)$ , the part of the Outcome not overlapping (light red area), should actually be assessed. In the worst case, the Mask Information is entirely contained in the Outcome (b). Separating the information in the imputed image  $x'_i$  and the mask  $M$  allows to reduce the overlap and the influence (c).

important features as an input. We suppose that there are inverse functions  $\mathcal{I}_{l,M}^{-1}$  and  $\mathcal{I}_{l,x}^{-1}$ , such that

$$x'_i = \mathcal{I}_l(M, x_i) \Leftrightarrow M = \mathcal{I}_{l,M}^{-1}(x'_i) \wedge x_i = \mathcal{I}_{l,x}^{-1}(x'_i).$$

If, for instance, the pixels removed are set to some reserved value indicating their absence, the imputation operator is invertible. Therefore,  $H(M|x'_i) = H(\mathcal{I}_{l,M}^{-1}(x'_i)|x'_i) = 0$ . In this case, also the Mitigator  $I(C; M|x'_i) = 0$ , because it is bounded by  $0 = H(M|x'_i) \geq I(C; M|x'_i) \geq 0$ . The ‘‘Feature Info’’ term is constrained to be positive. Thus, the Mask Information has a non-negligible impact on the ‘‘Evaluation Outcome’’, because a higher Mask Information term will always increase it. This case is depicted in Figure 4b.

We can create a simple example that shows how evaluation scores are influenced: Imagine a two-class problem that consists of detecting whether an object is located on the left or the right side of an image. A reasonable attribution method masks out pixels on the left or the right depending on the location of the object. In this case, the retraining step can lead to a classifier that infers the class just from the location of the masked out pixels and obtain high accuracy. This explanation map will be rated far worse in MoRF (no accuracy drop) than it might actually be. In Section 5.1, we empirically show that the leakage is significant for real data.

### 4.3. Reduction of Information Leakage

To solve this problem, we follow an intuitive approach: If we cannot guarantee that there is no class information contained in the mask itself, we have to stop it from leaking into the imputed images. Therefore, we make sure that the mask used cannot be easily inferred from the imputed version. We would like to set  $I(x'_i; M) = 0$ , i.e., the mask is independent of the imputed vector allowing to separate

the effects as shown in Figure 4c. Unfortunately, this is not possible in general: If both should be dependent on the class label, they will also have to share a minimal amount of information (that regarding the class). However, we can demand conditional independence and make  $I(x'_i; M)$  as small as possible.

**Condition 4.2. Minimally Revealing Imputation.** Let  $\mathcal{I}_l : \{0, 1\}^d \times \mathbb{R}^{d-k} \rightarrow \mathbb{R}^d$  be the infilling operator that takes the least important features as an input. Suppose  $x'_i$  and  $M$  are independent given the class information  $I(x'_i; M|C) = 0$  and  $I(x'_i; M) \approx 0$

In this case,  $I(C; M) - I(C; M|x'_i) = I(x'_i; M) - I(x'_i; M|C) \approx 0$ , which implies  $I(C; M) \approx I(C; M|x'_i)$  (also cf. Figure 4a again), indicating that the Mitigator effectively compensates the Mask Information term.

## 5. Debiasing Evaluation Strategies for Local Attribution Methods

In this section, we first show the impact of Class Information Leakage introduced in Section 4.2 on a real-world data set to highlight the necessity to compensate for this confounder. Building on the derivations in Section 4.3, we explain how we reduce its influence by proposing a novel imputation operator termed *Noisy Linear Imputation*.

### 5.1. Extent of Class Information Leakage

To empirically confirm our findings, we performed experiments on CIFAR-10 (Krizhevsky et al., 2009). We use the same attribution methods as in Hooker et al. (2019): Integrated Gradients (IG) (Sundararajan et al., 2017) and Guided Backprop (GB) (Springenberg et al., 2015) serve as base explanations, and three ensembling strategies for each are used in addition: SmoothGrad (SG) (Smilkov et al., 2017), SmoothGrad<sup>2</sup> (SQ) (Hooker et al., 2019) and

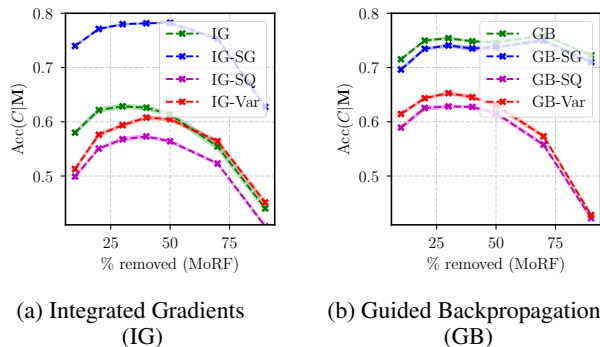


Figure 5. Accuracy of a trained classifier only using the binary masks  $\mathcal{M}$  without feature values as input on the CIFAR-10 data set. Binary masks  $\mathcal{M}$  were computed for different variants of IG and GB. Only the masks contain enough information to reach an accuracy of almost up to 80 % (compared to 85 % with full images) highlighting that the feature values do not play an important role in the evaluation. This underlines the necessity to compensate for this confounder.

VarGrad (Var) (Adebayo et al., 2018). In total, we consider eight attribution methods and provide details and parameters in the supplementary material.

We empirically show that with fixed value imputation with the global mean, the explanation masks are leaking class information. This takes two steps: (1) We show that the Mask Information  $I(C; \mathcal{M})$  is extremely high. (2) We verify that the Mitigator is small and cannot compensate the Mask Information, which completes our claim.

To assess the class information in the mask, we train a ResNet-18 (He et al., 2016) that uses only binary masks  $\mathcal{M}$  (no pixel values  $x_l$ ) to predict the class. The curves<sup>1</sup> are shown in Figure 5. Stuningly, the mask alone results in high accuracy curves that reach almost 80 % for IG-SG, only some percent below the accuracy of the classifier on the full inputs. This allows us to conclude that the Mask Information  $I(C; \mathcal{M})$  is almost as high as our Evaluation Outcome  $I(C; x_l')$ .

To show that the Mitigator is almost zero, we test the *Invertible Imputation* condition. Therefore, the inverse function  $\mathcal{I}_{l, \mathcal{M}}^{-1}$  that predicts the imputation mask from the imputed image is required (having this function, finding  $\mathcal{I}_{l, x}^{-1}$  is trivial). For the fixed value imputation, an approximate inverse is simple: Setting all pixels in the mask to 0 if the corresponding image pixel has the filling value (which has to be inferred from the distribution). For a stronger verification, we train an imputation predictor network consisting of three convolutional layers, which predicts for each pixel if it was imputed or original. As Figure 6e (blue curve) shows, the

<sup>1</sup>Standard Errors are indicated by shaded areas in all figures. However, they are often hardly visible due to their low magnitude.

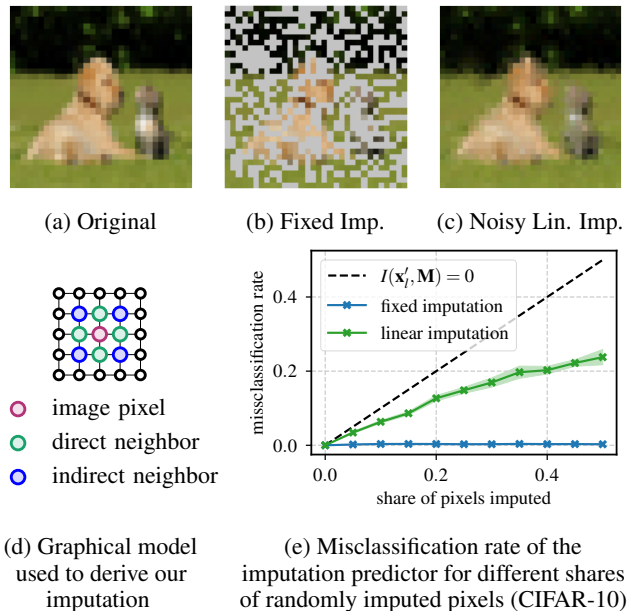


Figure 6. The considered imputation operators. When 50 % of the original image (a) are removed, they can either be imputed by a fixed value (b) or by our proposed Noisy Linear strategy (c,d). Training of an imputation predictor (e) shows that it is much harder to tell which pixels are original and which were imputed when using our proposed imputation model, which is closer to the theoretical optimum (black). Hence, by using imputed samples of this kind, Class Information Leakage is reduced.

miss-classification rate when using fixed value imputation is almost zero, i.e., the network can easily recognize the pixels that were imputed. According to our analysis, in this setting close to *Invertible Imputation*, the Mitigator will be negligibly small.

This leads us to the conclusion, that the mask-related leakage fundamentally influences many previous evaluations that use fixed value imputation (Shrikumar et al., 2017; Petsiuk et al., 2018; Hooker et al., 2019) and it is essential to stop the information leaking from the masks.

## 5.2. Debiasing with Noisy Linear Imputation

To reduce the Class Information Leakage, we propose a better-suited imputation operator  $\mathcal{I}_l$  that adheres to the *Minimally Revealing Imputation* condition we derived. The remaining process is left unchanged and stays as depicted in Figure 2. However, we face three requirements: (1) We have to get closer to the theoretical condition of Minimally Revealing Imputation. (2) The imputation strategy needs to be highly efficient, since the imputation module has to be run for each image in the data set. (3) We wish to have as few hyper-parameters as possible (preferably none to rule out another confounding factor).

We devised a new strategy called *Noisy Linear Imputation*,

which fulfills the above goals. In this way, our model addresses some of the most fundamental problems of existing strategies. Intuitively, we search a way to make more subtle imputations that cannot be easily recognized and result in lower  $I(\mathbf{x}'_j; \mathbf{M})$ . We suppose that each pixel can be approximated by the weighted mean of its neighbors (cf. Figure 6d) as image pixels are highly correlated<sup>2</sup>:

$$\mathbf{x}_{i,j} = w_d (\mathbf{x}_{i,j+1} + \mathbf{x}_{i,j-1} + \mathbf{x}_{i+1,j} + \mathbf{x}_{i-1,j}) + w_i (\mathbf{x}_{i+1,j+1} + \mathbf{x}_{i-1,j+1} + \mathbf{x}_{i+1,j-1} + \mathbf{x}_{i-1,j-1})$$

where  $w_d, w_i$  are constant coefficients for direct neighbors and indirect, diagonal neighbors. Setting up a single equation for each removed pixel, we arrive at an equation system, where the number of unknowns is the same as the number of pixel values removed. The system is sparse and can be efficiently solved, even for a large number of missing pixels. To choose the neighbor weights for the linear interpolation, we draw inspiration from the graph structure: Indirect neighbors have distance 2 from the original node in the graph and direct neighbors have distance 1. Hence, we gave the direct neighbors twice the weight of the diagonal ones. Because the weights need to sum up to 1 for a weighted interpolation, this leads to  $w_d = \frac{1}{6}$  and  $w_i = \frac{1}{12}$ . We add a small random noise ( $\sigma = 0.1$ ) to the solution to ensure that the linear dependency cannot be learned by the model.

Figure 6 (top) provides an example of an imputed sample. From the imputed version in Figure 6c, inference on the mask is significantly harder than the one imputed with fixed values as in Figure 6b. We again train the imputation predictor for verification and show the results in Figure 6e. We confirm that our strategy lies significantly closer to the optimal, Minimally Revealing Imputation. Admittedly, there are even more sophisticated imputation strategies, for example building on Generative Adversarial Networks (GANs), e.g., by (Yoon et al., 2018). However, our strategy already achieves considerable improvements and is highly efficient, so we leave the task of finding an optimal strategy to future work.

## 6. Experiments

Having established that our Noisy Linear Imputation fulfills its purpose, in this section, we show its advantages in practice. We first highlight how it makes results among different evaluation strategies more consistent in Section 6.1. We then present another considerable advantage in Section 6.2: its agreement with a no-retraining evaluation strategy is sufficiently high, that the retraining step is no longer required. We name this debiased and no-retraining evaluation framework ROAD (RemOve And Debias). All experiments were conducted on CIFAR-10 using the eight

<sup>2</sup>In fact, for direct and indirect neighbors,  $\rho=0.89$  and  $\rho=0.82$  respectively on CIFAR-10

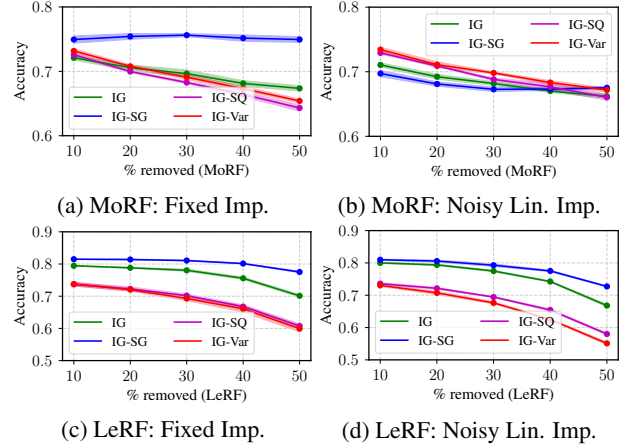


Figure 7. Consistency comparison using fixed value vs. Noisy Linear Imputation. The higher accuracy is better in LeRF, while the lower is better in MoRF. Comparing (a) and (c), fixed value imputation gives different rankings in MoRF and LeRF orders: IG-SG is the best in LeRF but the worst in MoRF. Comparing (b) and (d), Noisy Linear Imputation changes the outcome considerably and yields a consistent ranking in MoRF and LeRF.

attribution methods mentioned in the last section.

### 6.1. Consistency under Removal Orders

As we aim for evaluation strategies that are less prone to the hyperparameter setting and allow for a consistent ranking, we study the consistency of evaluation results under different removal orders MoRF and LeRF. Figure 7 depicts the obtained curves. For a clear view, we only show four curves of attribution methods based on IG with retraining and up to 50% pixels are removed. We include the full curves for the IG with its derivatives as well as GB with derivatives in our Appendix B. The results using the common fixed value imputation shown in Figure 7 (a) and (c). The results with our Noisy Linear Imputation are shown in (b) and (d). In MoRF, a sharp drop in the beginning indicates a better attribution method, while a slight drop is desirable in LeRF. Hence, using fixed imputation, the ranking in MoRF is IG, IG-Var, IG-SQ, IG-SG, whereas the ranking in LeRF is IG-SG, IG, IG-SQ, and IG-Var. We see, for instance, that IG-SG is the worst in MoRF and the best in LeRF. When using the Noisy Linear Imputation, the inconsistency vanishes. The ranking in MoRF is: IG-SG, IG, IG-SQ, and IG-Var, which is the same as in LeRF.

We quantitatively compute the consistency among all eight attribution methods with and without retraining. Concretely, we compute the ranks (from 1=best to 8=worst) of our explanation methods for each percentage of perturbed pixels. We then calculate the Spearman Rank correlation between different evaluation strategies. As shown in Table 2, the correlation score of the fixed value imputation is  $-0.05$  when using retraining and  $0.01$  when no retraining is applied.

Retrain		No-Retrain	
MoRF vs. LeRF		MoRF vs. LeRF	
fixed	lin	fixed	lin
-0.09±0.01	<b>0.59±0.01</b>	0.01±0.01	<b>0.54±0.01</b>

Table 2. Spearman rank correlation between evaluation strategies. There is almost no agreement between MoRF and LeRF when using fixed imputation (as in previous works). When using our imputation (“lin”), consistency across MoRF and LeRF orders increases drastically.

This indicates no consistency in the rankings. When we deploy our Noisy Linear Imputation, the results change drastically: The correlation score is improved to 0.59 and 0.54 with and without retraining, respectively. This also implies that the information leakage is responsible for a major share of the inconsistency.

## 6.2. Efficiency

When we apply our Noisy Linear Imputation, we additionally reduce the difference between evaluation with and without retraining. This can be attributed to the reduced distribution shift incurred when using an almost *Minimally Revealing Imputation*. If all pixels were perfectly imputed, the resulting image would not be out-of-distribution. Since we are interested in the rankings of attribution methods, we again compute Spearman correlation between the rankings obtained with and without retraining and show it in Table 3. The order remains almost always intact between the “Retrain” with Noisy Linear Imputation and the “No-Retrain” variant with Noisy Linear Imputation resulting in a rank correlation of 0.86 in using MoRF and 0.95 in LeRF. This leads us to the conclusion that “No-Retrain” and “Retrain” end up with a highly similar ranking when using Noisy Linear Imputation. Thus, we conclude that the retraining step is not longer justified and can be skipped without significant distortion of the results.

These results allow us to introduce a novel evaluation framework. We refer to the removal with Noisy Linear Imputation and no retraining as ROAD – Remove and Debias. We showed that ROAD is highly consistent with

MoRF		LeRF	
Retain vs. No-Retr.		Retain vs. No-Retr.	
fixed	lin	fixed	lin
0.14±0.02	<b>0.86±0.01</b>	0.05±0.01	<b>0.95±0.01</b>

Table 3. Spearman rank correlation between evaluation with and without retraining. Our Noisy Linear Imputation (“lin”) also results only in marginal differences between “Retrain” and “No-Retrain”. We conclude that the retraining step is no longer necessary.

Strategy	Retrain		No-Retrain	
	fixed <sup>†</sup>	lin	fixed	lin <sup>*</sup>
Time	5986±5 s	6412±13 s	33.8±0.3 s	42.3±0.2 s
Relative	100 %	107 %	0.6 %	0.7 %

Table 4. Mean runtime (5 runs) for evaluating a single explanation method (IG). <sup>†</sup> refers to ROAR, and <sup>\*</sup> to our ROAD.

the compensated results of the ROAR, but comes at an enormous advantage: The retraining step is no longer required. This permits to save a vast amount of computation time. In our experiments, evaluation using the ROAD took only 0.7 % of the resources required for ROAR, as given by the runtimes in Table 4 obtained on the same hardware (single Nvidia GTX 2080Ti and 8 Cores).

In the end, we illustrate the evaluation results using ROAD among all eight attribution methods in MoRF and LeRF in Figure 8. In MoRF, the best ones are IG-SG, GB-SQ, GB-Var and IG, which have lower accuracies in the beginning, whereas they have higher accuracies in LeRF. GB and GB-Var both perform badly in MoRF and LeRF. We see that some inconsistencies still remain, which cannot be compensated by the current imputation. However, the evaluation strategies might also consider different characteristics of an attribution method (e.g., one might be particularly good at identifying irrelevant pixels), which is why perfect agreement might not even be desirable.

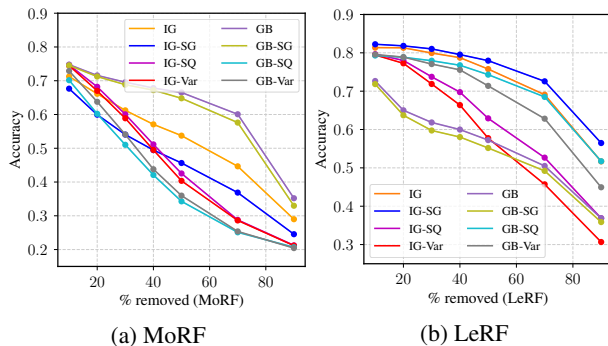


Figure 8. Evaluation results in MoRF (a) and LeRF (b) using our ROAD framework.

## 7. Conclusion and Outlook

We introduced ROAD, an evaluation approach for measuring global fidelity among attribution explanations. ROAD comes with two key advantages over existing methods: (1) it is highly efficient, e.g., permitting a 99% runtime reduction w.r.t. ROAR, and (2) it circumvents the Class Information Leakage issue, which was thoroughly analyzed in this work. We believe the ROAD framework will be beneficial to the research community because it unifies several methods and is more consistent under varying



removal orders. Moreover, it is broadly accessible due to its low resource requirements, it is open-source, and can be readily implemented in practical use-cases. Going forward, we plan to investigate more sophisticated imputation models in ROAD as well as other evaluation metrics besides fidelity.

## References

- Adadi, A. and Berrada, M. Peeking inside the black-box: a survey on explainable artificial intelligence (xai). *IEEE access*, 6:52138–52160, 2018.
- Adebayo, J., Gilmer, J., Muelly, M., Goodfellow, I., Hardt, M., and Kim, B. Sanity checks for saliency maps. In *Advances in Neural Information Processing Systems*, volume 31, 2018.
- Adebayo, J., Muelly, M., Liccardi, I., and Kim, B. Debugging tests for model explanations. *arXiv preprint arXiv:2011.05429*, 2020.
- Afchar, D. and Hennequin, R. Making neural networks interpretable with attribution: application to implicit signals prediction. In *Fourteenth ACM Conference on Recommender Systems*, pp. 220–229, 2020.
- Afchar, D., Guigue, V., and Hennequin, R. Towards rigorous interpretations: a formalisation of feature attribution. In *International Conference on Machine Learning*, pp. 76–86. PMLR, 2021.
- Ancona, M., Ceolini, E., Öztireli, C., and Gross, M. Towards better understanding of gradient-based attribution methods for deep neural networks. *arXiv preprint arXiv:1711.06104*, 2017.
- Bach, S., Binder, A., Montavon, G., Klauschen, F., Müller, K.-R., and Samek, W. On pixel-wise explanations for non-linear classifier decisions by layer-wise relevance propagation. *PLoS one*, 10(7):e0130140, 2015.
- Bhatt, U., Weller, A., and Moura, J. M. Evaluating and aggregating feature-based model explanations. In *Proceedings of the Twenty-Ninth International Joint Conference on Artificial Intelligence*, pp. 3016–3022, 2020a.
- Bhatt, U., Xiang, A., Sharma, S., Weller, A., Taly, A., Jia, Y., Ghosh, J., Puri, R., Moura, J. M., and Eckersley, P. Explainable machine learning in deployment. In *Proceedings of the 2020 Conference on Fairness, Accountability, and Transparency*, pp. 648–657, 2020b.
- Chen, J., Song, L., Wainwright, M. J., and Jordan, M. I. L-shapley and c-shapley: Efficient model interpretation for structured data. In *International Conference on Learning Representations*, 2018.
- Cover, T. M. and Thomas, J. A. *Elements of Information Theory*. John Wiley and Sons, 2006. doi: 10.1002/047174882X.
- Doshi-Velez, F. and Kim, B. Towards a rigorous science of interpretable machine learning. *arXiv preprint arXiv:1702.08608*, 2017.
- Eitel, F., Ritter, K., Alzheimer’s Disease Neuroimaging Initiative (ADNI), et al. Testing the robustness of attribution methods for convolutional neural networks in mri-based alzheimer’s disease classification. In *Interpretability of Machine Intelligence in Medical Image Computing and Multimodal Learning for Clinical Decision Support*, pp. 3–11. Springer, 2019.
- Fel, T., Vigouroux, D., Cadène, R., and Serre, T. How good is your explanation? algorithmic stability measures to assess the quality of explanations for deep neural networks. 2021.
- Fong, R. C. and Vedaldi, A. Interpretable explanations of black boxes by meaningful perturbation. In *Proceedings of the IEEE international conference on computer vision*, pp. 3429–3437, 2017.
- Hartley, T., Sidorov, K., Willis, C., and Marshall, D. Explaining failure: Investigation of surprise and expectation in cnns. In *Proceedings of the IEEE/CVF Conference on Computer Vision and Pattern Recognition Workshops*, pp. 12–13, 2020.
- Hase, P. and Bansal, M. Evaluating explainable AI: Which algorithmic explanations help users predict model behavior? In *Proceedings of the 58th Annual Meeting of the Association for Computational Linguistics*, pp. 5540–5552, 2020.
- Haug, J., Zürn, S., El-Jiz, P., and Kasneci, G. On baselines for local feature attributions. *AAAI Workshop on Explainable Agency in AI Workshop*, 2021.
- He, K., Zhang, X., Ren, S., and Sun, J. Deep residual learning for image recognition. In *Proceedings of the IEEE conference on computer vision and pattern recognition*, pp. 770–778, 2016.
- Hellman, M. E. and Raviv, J. Probability of Error, Equivocation, and the Chernoff Bound. *IEEE Transactions on Information Theory*, 16(4):368–372, 1970.
- Hooker, S., Erhan, D., Kindermans, P. J., and Kim, B. A benchmark for interpretability methods in deep neural networks. In *Advances in Neural Information Processing Systems*, volume 32, 2019.

- Izzo, C., Lipani, A., Okhrati, R., and Medda, F. A baseline for shapely values in mlps: from missingness to neutrality. *arXiv preprint arXiv:2006.04896*, 2020.
- Kasneji, G. and Gottron, T. Licon: A linear weighting scheme for the contribution of input variables in deep artificial neural networks. In *Proceedings of the 25th ACM International on Conference on Information and Knowledge Management*, pp. 45–54, 2016.
- Krizhevsky, A., Hinton, G., et al. Learning multiple layers of features from tiny images. 2009.
- Lundberg, S. M. and Lee, S.-I. A unified approach to interpreting model predictions. In *Proceedings of the 31st international conference on neural information processing systems*, pp. 4768–4777, 2017.
- Meng, C., Trinh, L., Xu, N., and Liu, Y. Mimic-iv: Interpretability and fairness evaluation of deep learning models on mimic-iv dataset. *arXiv preprint arXiv:2102.06761*, 2021.
- Meyen, S. Relation between classification accuracy and mutual information in equally weighted classification task. Master’s thesis, University of Hamburg, 2016. URL <https://osf.io/zru7b/>.
- Nauta, M., Trienes, J., Pathak, S., Nguyen, E., Peters, M., Schmitt, Y., Schlötterer, J., van Keulen, M., and Seifert, C. From anecdotal evidence to quantitative evaluation methods: A systematic review on evaluating explainable ai. *arXiv preprint arXiv:2201.08164*, 2022.
- Nguyen, A. P. and Martínez, M. R. On quantitative aspects of model interpretability. *arXiv preprint arXiv:2007.07584*, 2020.
- Petsiuk, V., Das, A., and Saenko, K. Rise: Randomized input sampling for explanation of black-box models. In *Proceedings of the British Machine Vision Conference (BMVC)*, 2018.
- Ribeiro, M. T., Singh, S., and Guestrin, C. ” why should i trust you?” explaining the predictions of any classifier. In *Proceedings of the 22nd ACM SIGKDD international conference on knowledge discovery and data mining*, pp. 1135–1144, 2016.
- Samek, W., Binder, A., Montavon, G., Lapuschkin, S., and Müller, K.-R. Evaluating the visualization of what a deep neural network has learned. *IEEE transactions on neural networks and learning systems*, 28(11):2660–2673, 2016.
- Schramowski, P., Stammer, W., Teso, S., Brugger, A., Herbert, F., Shao, X., Luigs, H.-G., Mahlein, A.-K., and Kersting, K. Making deep neural networks right for the right scientific reasons by interacting with their explanations. *Nature Machine Intelligence*, 2(8):476–486, 2020.
- Selvaraju, R. R., Cogswell, M., Das, A., Vedantam, R., Parikh, D., and Batra, D. Grad-cam: Visual explanations from deep networks via gradient-based localization. In *Proceedings of the IEEE international conference on computer vision*, pp. 618–626, 2017.
- Shah, H., Jain, P., and Netrapalli, P. Do input gradients highlight discriminative features?, 2021.
- Shrikumar, A., Greenside, P., and Kundaje, A. Learning important features through propagating activation differences. In *International Conference on Machine Learning*, pp. 3145–3153. PMLR, 2017.
- Smilkov, D., Thorat, N., Kim, B., Viégas, F., and Wattenberg, M. Smoothgrad: removing noise by adding noise. In *Workshop on Visualization for Deep Learning, ICML*, 2017.
- Springenberg, J. T., Dosovitskiy, A., Brox, T., and Riedmiller, M. Striving for simplicity: The all convolutional net. In *ICLR (workshop track)*, 2015.
- Srinivas, S. and Fleuret, F. Full-gradient representation for neural network visualization. In *Advances in Neural Information Processing Systems (NeurIPS)*, 2019.
- Sturmfels, P., Lundberg, S., and Lee, S.-I. Visualizing the impact of feature attribution baselines. *Distill*, 5(1):e22, 2020.
- Sundararajan, M., Taly, A., and Yan, Q. Axiomatic attribution for deep networks. In *International Conference on Machine Learning*, pp. 3319–3328. PMLR, 2017.
- Sutskever, I., Martens, J., Dahl, G., and Hinton, G. On the importance of initialization and momentum in deep learning. In *International conference on machine learning*, pp. 1139–1147. PMLR, 2013.
- Tjoa, E. and Guan, C. A survey on explainable artificial intelligence (xai): Toward medical xai. *IEEE Transactions on Neural Networks and Learning Systems*, 2020.
- Tomsett, R., Harborne, D., Chakraborty, S., Gurram, P., and Preece, A. Sanity checks for saliency metrics. In *Proceedings of the AAAI Conference on Artificial Intelligence*, volume 34, pp. 6021–6029, 2020.
- Vergara, J. R. and Estévez, P. A. A review of feature selection methods based on mutual information. *Neural Computing and Applications*, 24(1):175–186, 2014. ISSN 09410643. doi: 10.1007/s00521-013-1368-0.

Xu, S., Venugopalan, S., and Sundararajan, M. Attribution in scale and space. In *Proceedings of the IEEE/CVF Conference on Computer Vision and Pattern Recognition*, pp. 9680–9689, 2020.

Yeh, C.-K., Hsieh, C.-Y., Suggala, A., Inouye, D. I., and Ravikumar, P. K. On the (in) fidelity and sensitivity of explanations. *Advances in Neural Information Processing Systems*, 32:10967–10978, 2019.

Yoon, J., Jordon, J., and Schaar, M. Gain: Missing data imputation using generative adversarial nets. In *International Conference on Machine Learning*, pp. 5689–5698. PMLR, 2018.

## A. Additional Theory

### A.1. Formulation of the MI Bounds for the Binary Case

As we discussed in our main paper, the relationship between Mutual Information (MI) and accuracy is not a function, but comes in form of upper and lower bounds of the obtainable accuracy. If, for example, the binary classification case with equal class priors  $p(C = 0) = p(C = 1) = \frac{1}{2}$  is considered, the following bounds can be derived (Hellman & Raviv, 1970; Meyen, 2016):

$$\frac{I(\mathbf{x}; C) + 1}{2} \leq \text{Acc}(C|\mathbf{x}) \leq H_2^{-1}(1 - I(\mathbf{x}; C)), \quad (3)$$

where  $H_2^{-1} : [0, 1] \rightarrow [\frac{1}{2}, 1]$  is the inverse of the binary entropy with support  $[\frac{1}{2}, 1]$ . For completeness, we restate the proof of this upper bound in Appendix A.2.

### A.2. Reproduction of the proof of the relation between mutual and accuracy in the binary case

In this section, we reproduce the proofs for the upper and lower bounds of bayesian classifier accuracy given a certain amount of mutual information from the master's thesis by (Meyen, 2016) for completeness. The upper bound given there is tighter than the bounds present in the literature.

We consider the following setting ( $C, \mathbf{x}$  are random variables):

- binary classification problem,  $C \in \Omega_C = \{0, 1\}$
- equal class priors  $P(C = 0) = \frac{1}{2}, P(C = 1) = \frac{1}{2}$
- discrete features  $\mathbf{x}$  (which can be the product of multiple random variables)
- support set  $\Omega_x = \text{supp}\{\mathbf{x}\}$  of *countable* size

We first prove the following Lemma:

**Lemma A.1.** *Let the assumptions stated above be true. Then, the mutual information is the weighted mean of a function of the conditional accuracies  $\text{Acc}(C|s)$ , where  $s \in \Omega_x$ :*

$$I(C; \mathbf{x}) = \sum_{s \in \Omega_x} p(s) (1 - H_2[\text{Acc}(C|s)])$$

In this formulation,  $p(s)$  is a shorthand for  $P(\mathbf{x} = s)$  and  $H_2(p) := -p \log p - (1 - p) \log(1 - p)$  is the entropy for a binary random variable.

**Proof.**

$$I(C; \mathbf{x}) = H(C) - H(C|\mathbf{x}) \quad (4)$$

$$= \sum_{c \in \Omega_C} p(c) \log \frac{1}{p(c)} - \sum_{s \in \Omega_x} p(s) \sum_{c \in \Omega_C} p(c|s) \log \frac{1}{p(c|s)} \quad (5)$$

$$= \sum_{s \in \Omega_x} p(s) \left[ \sum_{c \in \Omega_C} p(c) \log \frac{1}{p(c)} - \sum_{c \in \Omega_C} p(c|s) \log \frac{1}{p(c|s)} \right] \quad (6)$$

$$= \sum_{s \in \Omega_x} p(s) [H(C) - H(C|s)] \quad (7)$$

In our consideration,  $\Omega_C = \{0, 1\}$  and  $P(C = 0) = \frac{1}{2}, P(C = 1) = \frac{1}{2}$ , so  $H(C) = 1$ . Additionally, the bayesian classifier rule yields

$$\text{acc}(C|s) = \begin{cases} P(C = 0|s), & \text{for } P(C = 1|s) \leq 0.5 \\ P(C = 1|s), & \text{for } P(C = 1|s) > 0.5 \end{cases} \quad (8)$$

and

$$H(C|s) = -P(C = 0|s) \log P(C = 0|s) - P(C = 1|s) \log P(C = 1|s) \quad (9)$$

$$= H_2(P(C = 0|s)) = H_2(P(C = 1|s)) \quad (10)$$

$$= H_2(\text{acc}(C|s)) \quad (11)$$

Plugging in the results  $H(C) = 1$  and  $H(C|s) = H_2(\text{Acc}(C|s))$ , we obtain the proposed lemma.  $\square$

For the derivation of upper and lower bounds, Jenssen’s inequality is used.  $1 - H_2(\cdot)$  is a convex function and the  $\{p(s)\}_{s \in \Omega_x}$  are convex multipliers, i.e., they are non-negative and sum up to one. Then,

$$1 - H_2(\text{Acc}(C|\mathbf{x})) = 1 - H_2\left(\sum_{s \in \Omega_x} p(s) \text{Acc}(C|s)\right) \quad (12)$$

$$\leq \sum_{s \in \Omega_x} p(s) [1 - H_2(\text{Acc}(C|s))] = I(\mathbf{x}; C) \quad (13)$$

We can restate this equation in terms of accuracy.

$$H_2(\text{Acc}(C|\mathbf{x})) \geq 1 - I(C; \mathbf{x}) \quad (14)$$

Using that  $H_2(\cdot)$  is decreasing monotonically on the interval  $[\frac{1}{2}, 1]$ , so its inverse  $H_2^{-1}$  exists, and that  $\text{Acc}(C|s) \geq 0.5$ :

$$\text{Acc}(C|\mathbf{x}) \leq H_2^{-1}(1 - I(C; \mathbf{x})). \quad (15)$$

The inequality sign is flipped again, due to the inverse being monotonically decreasing. Note that the bounds derived for the special case are much tighter than the general ones provided by Vergara & Estévez (2014) and Cover & Thomas (2006, Chapter 2.10), that are not of any use, because they are even less strict than the trivial bound  $\text{Acc}(C|\mathbf{x}) \leq 1$ , for the simple case considered here.

For the lower bound, we refer the reader to Hellman & Raviv (1970, eqn. 18), where the term  $I$  corresponds to  $H(C|\mathbf{x}) = H(C) - I(C; \mathbf{x})$  in our notation. Rewriting the result from Hellman & Raviv (1970) in our notation, we obtain

$$1 - \text{Acc}(C|\mathbf{x}) \leq \frac{H(C) - I(C; \mathbf{x})}{2}. \quad (16)$$

Using  $H(C) = 1$  and rearranging yields

$$1 - \text{Acc}(C|\mathbf{x}) \leq \frac{1 - I(C; \mathbf{x})}{2} \quad (17)$$

and

$$\text{Acc}(C|\mathbf{x}) \geq \frac{I(C; \mathbf{x}) + 1}{2}. \quad (18)$$

$\square$

### A.3. Analysis of the LeRF Ordering

In this section, we analyze the masking impact for the case of the Least Relevant First (LeRF) ordering. We first provide a definition for the operators involved as we did for the Most Relevant First (MoRF) case. In the LeRF setting, the  $k$  least important features per instance are removed. We model the explanation as a choice of features via a binary mask  $\mathbf{M} = e(f, \mathbf{x}) \in \{0, 1\}^d$ , with the corresponding value set to one, if the corresponding feature is among the top- $k$ , and to zero otherwise. Furthermore, suppose  $\mathcal{M}_h : \{0, 1\}^d \times \mathbb{R}^d \rightarrow \mathbb{R}^k$  to be the selection operator for the highly important dimensions indicated in the mask and  $\mathbf{x}_h = \mathcal{M}_h(\mathbf{M}, \mathbf{x})$  to be a vector containing only the remaining, highly important features as shown in Figure 9. We suppose that the features preserve their internal order in  $\mathbf{x}_h$ , i.e., features are ordered ascendingly by their original input indices.

The LeRF approach with retraining (also called “Keep and Retrain”, KAR, by Hooker et al. (2019)) measures the accuracy of a newly trained classifier  $f'$  on modified samples  $\mathbf{x}'_h := \mathcal{I}_h(\mathbf{M}, \mathbf{x}_h)$ , where  $\mathcal{I}_h : \{0, 1\}^d \times \mathbb{R}^k \rightarrow \mathbb{R}^d$  is an imputation

operator that redistributes all inputs in the vector  $\mathbf{x}_h$  to their original positions and sets the remainder to some filling value. This means only the top- $k$  features are kept. For a better evaluation result, the accuracy should increase quickly with increasing  $k$ , indicating the most influential features are present. Accuracy should not increase much for the high values of  $k$  because removing the low importance features should not have a large effect. Overall, higher accuracies indicate better explanations in the LeRF setting.

For the LeRF benchmark, the quantity of interest in our analysis will be  $I(\mathbf{x}'_h; C)$ , the class information contained in the filled-in version of the selected high important features. We want to maximize  $I(\mathbf{x}'_h; C)$  to obtain a good score,

$$\uparrow I(\mathbf{x}'_h; C) \Rightarrow \uparrow \text{LeRF benchmark.}$$

As before, we can apply the following, general identity:

$$\underbrace{I(\mathbf{x}'_h; C)}_{\text{Evaluation Outcome}} = \underbrace{I(C; \mathbf{x}'_h | M)}_{\text{Feature Info.}} + \underbrace{I(C; M)}_{\text{Mask Info.}} - \underbrace{I(C; M | \mathbf{x}'_h)}_{\text{Mitigator}}. \quad (19)$$

The interpretation of the terms is analogous to that in our main paper.

**Class-Leaking Explanation Map** For the case of the class-leaking map, we again require the imputation operator to be invertible:

**Example A.2. Invertible Imputation.** Let  $\mathcal{I}_h : \{0, 1\}^d \times \mathbb{R}^k \rightarrow \mathbb{R}^d$  be the imputation operator that takes the highly important features as an input. We suppose that there are inverse functions  $\mathcal{I}_{h,M}^{-1}$  and  $\mathcal{I}_{h,x}^{-1}$ , such that

$$\mathbf{x}'_h = \mathcal{I}_h(M, \mathbf{x}_h) \Leftrightarrow M = \mathcal{I}_{h,M}^{-1}(\mathbf{x}'_h) \wedge \mathbf{x}_h = \mathcal{I}_{h,x}^{-1}(\mathbf{x}'_h).$$

If, for instance, the pixels removed are set to some reserved value indicating their absence, the infilling operator is invertible. In this case, also the Mitigator  $I(C; M | \mathbf{x}'_h) = 0$  (see Section 4.3 for details). The ‘‘Feature Info’’ term is constrained to be positive. Thus, the Mask Information has a non-negligible impact on the Evaluation Goal, because a higher Mask term will always increase it.

We can create a another example of a spurious explanation map that shows how evaluation scores are influenced even worse for LeRF: Suppose an explanation map that starts masking out pixels at the top for class zero and at the bottom for class one. Thus, a retrained model will be able to infer the category just from the shape of the masked pixels and obtain the best possible accuracy and thus score in the LeRF setting. However, it does not provide a reasonable attribution for the importance of the features.

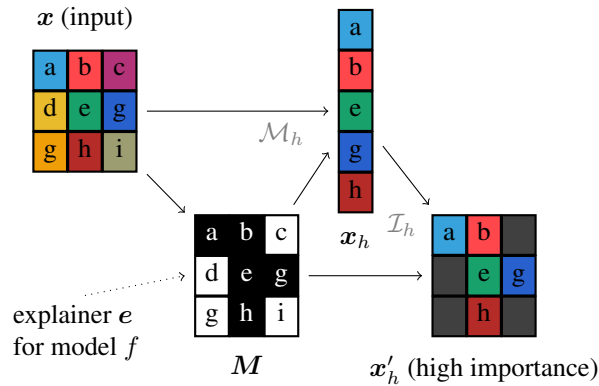


Figure 9. Analogous analytical model of feature removal in the opposite order (LeRF): The input image  $\mathbf{x}$  is explained by an explanation method that returns a mask  $M$  indicating important pixels. The remaining, highly important pixels can be extracted from the image using the masking operator  $\mathcal{M}_h$  and transformed to a modified variant of the input  $\mathbf{x}'_h$  via the imputation operator  $\mathcal{I}_h$ .

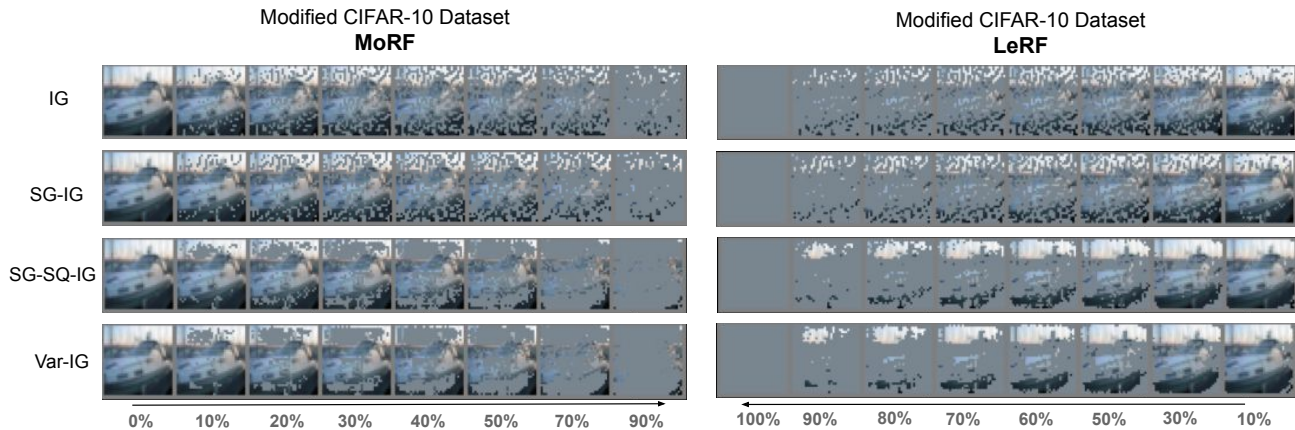


Figure 10. Illustration of modified data set in MoRF/LeRF and fixed value imputation settings. **Left:** Modifications in the MoRF framework. **Right:** Modifications in the LeRF framework. **Top to Bottom:** Modifications using Integrated Gradient (IG) (Sundararajan et al., 2017) and three ensemble variants of IG: SmoothGrad (SG-IG) (Smilkov et al., 2017), SmoothGrad<sup>2</sup> (SG-SQ-IG) (Hooker et al., 2019), and VarGrad (Var-IG) (Adebayo et al., 2018). The percentage of pixels that are removed or kept is given at the bottom.

## B. Experiments

### B.1. Implementation Details

We train a vanilla ResNet-18 He et al. (2016) on CIFAR-10 and compute different explanations using the trained model. The model is trained with the initial learning rate of 0.01 and the SGD optimizer Sutskever et al. (2013). We decrease the learning rate by factor 0.1 after 25 and train the model for 40 epochs on one (Nvidia RTX 3090) GPU. The trained model achieves a test set accuracy of 84.5% (comparable to the model in Tomsett et al. (2020)). For attributions, we use the same settings as in (Hooker et al., 2019): As base explanations we implement Integrated Gradient (IG) (Sundararajan et al., 2017) and Guided Backprop (GB) (Springenberg et al., 2015). Additionally, we use three ensembling strategies for each: SmoothGrad (SG) (Smilkov et al., 2017), SmoothGrad<sup>2</sup> (SG-SQ) (Hooker et al., 2019) and VarGrad (Var) (Adebayo et al., 2018). For each explanation method, we modify the data set using the fraction of pixels  $\eta = [0, 0.1, 0.2, 0.3, 0.4, 0.5, 0.7, 0.9]$ . Figure 10 illustrates the modified images by using four different explanations in the GB-family within MoRF and LeRF orders (fixed mean value imputation is used).

We use  $N = 5$  runs and report averaged results for all CIFAR-10 experiments in our paper and indicate the standard errors (which are very small) as an area behind our plots. In Table 5 and Table 6, we show the mean accuracy and its standard deviation at each the fraction of pixels  $\eta$  for IG-SG and GB-SG explanations. For other explanations we used, the standard deviation at each  $\eta$  in the magnitude of below one percent as well.

		10	20	30	40	50	70	90
Retrain MoRF	fix	74.94±0.57	75.42±0.45	75.62±0.24	75.16±0.50	74.95±0.45	73.73±0.48	65.18±0.85
	lin*	69.72±0.49	68.10±0.34	67.28±0.34	67.32±0.22	67.52±0.22	66.46±0.54	60.37±0.51
No-Retrain MoRF	fix	44.06±0.04	29.81±0.03	21.99±0.03	17.35±0.02	14.67±0.01	11.50±0.04	10.90±0.03
	lin*	67.66±0.02	59.94±0.03	54.05±0.05	49.46±0.04	45.63±0.06	36.87±0.05	24.55±0.04
Retrain LeRF	fix	77.52±0.26	80.14±0.11	81.08±0.14	81.40±0.15	81.50±0.07	81.85±0.12	82.01±0.20
	lin*	72.73±0.20	77.52±0.23	79.29±0.41	80.57±0.31	80.97±0.20	81.64±0.26	81.41±0.13
No-Retrain LeRF	fix	46.76±0.04	51.84±0.04	53.80±0.05	55.39±0.06	57.59±0.05	64.02±0.05	74.33±0.03
	lin*	56.48±0.03	72.57±0.03	77.96±0.02	79.54±0.01	81.02±0.04	81.82±0.02	82.24±0.01

Table 5. Mean accuracy at each  $\eta$  by using IG-SG in all methods with standard deviations of five individual runs. For LeRF, the accuracy is at  $(1-\eta)$ .

### B.2. Extended Figures

In this section, we include more results when comparing fixed value imputation and our proposed Noisy Linear Imputation. In Figure 13, the full plots of IG-family attribution methods with retraining in MoRF and LeRF are shown, while Figure 12

## Evaluating Feature Attribution: An Information-Theoretic Perspective

		10	20	30	40	50	70	90
Retrain MoRF	fix	76.30±0.43	75.60±0.27	74.89±0.29	74.27±0.29	73.37±0.28	72.15±0.09	67.99±0.24
	lin*	72.83±0.37	71.87±0.41	71.58±0.19	70.98±0.15	70.47±0.20	67.81±0.45	59.38±0.46
No-Retrain MoRF	fix	73.01±0.04	66.73±0.04	58.69±0.09	52.47±0.10	48.52±0.05	48.71±0.04	44.39±0.01
	lin*	74.54±0.03	71.24±0.04	68.83±0.02	67.21±0.01	64.80±0.04	57.60±0.08	32.98±0.03
Retrain LeRF	fix	66.97±0.52	70.45±0.30	71.44±0.25	72.15±0.15	72.72±0.11	73.91±0.19	75.24±0.25
	lin*	59.88±0.39	65.42±0.47	67.76±0.53	68.59±0.19	69.42±0.67	69.90±0.30	72.13±0.40
No-Retrain LeRF	fix	37.12±0.03	41.63±0.03	42.32±0.05	43.99±0.07	46.96±0.12	57.85±0.02	69.62±0.02
	lin*	35.87±0.04	49.21±0.04	55.18±0.08	58.04±0.03	59.75±0.02	63.71±0.04	71.85±0.02

Table 6. Mean accuracy at each  $\eta$  by using GB-SG in all methods with standard deviations of five individual runs. For LeRF, the accuracy is at  $(1-\eta)$ .

		Retrain MoRF		No-Retrain MoRF		Retrain LeRF		No-Retrain LeRF	
		fix <sup>†</sup>	lin	lin*	fix	fix	lin	lin	fix
Retrain MoRF	fix <sup>†</sup>	1.00							
	lin	±0.00							
No-Retrain MoRF	lin*	0.69	1.00						
	fix	±0.02	±0.00						
Retrain LeRF	fix	<b>0.65</b>	<b>0.86</b>	1.00					
	lin	±0.01	±0.01	±0.00					
No-Retrain LeRF	fix	<b>0.14</b>	0.41	0.45	1.00				
	lin	±0.02	±0.02	±0.01	±0.00				
Retrain MoRF	fix	<b>-0.09</b>	0.41	0.33	0.58	1.00			
	lin	±0.02	±0.02	±0.01	±0.01	±0.00			
No-Retrain MoRF	fix	0.14	<b>0.57</b>	0.52	0.74	0.86	1.00		
	lin	±0.01	±0.01	±0.01	±0.01	±0.01	±0.00		
Retrain LeRF	fix	0.19	0.59	<b>0.53</b>	0.79	0.82	<b>0.95</b>	1.00	
	lin	±0.01	±0.01	±0.01	±0.01	±0.01	±0.01	±0.00	
No-Retrain LeRF	fix	0.49	0.53	0.68	<b>0.01</b>	<b>0.05</b>	0.13	0.18	1.00
	lin	±0.01	±0.01	±0.01	±0.01	±0.01	±0.01	±0.01	±0.00

Table 7. Rank Correlations between all evaluation strategies used with standard deviations computed by considering the rankings obtained through five consecutive runs as independent. Results indicated in bold correspond to those reported in the main paper. The ROAR benchmark is marked by <sup>†</sup> and our ROAD by \*.

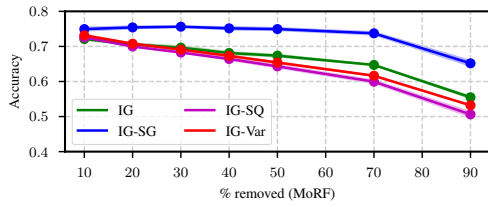
illustrates for the GB-based attribution methods. Figure 13 and Figure 14 show the evaluation results when no retraining is used in MoRF and LeRF for IG- and GB-family attribution methods, respectively. From results, we see that using our Noisy Linear Imputation, we increase the consistency between the evaluation rankings conducted in MoRF and LeRF with and without retraining.

### B.3. Correlation Analysis

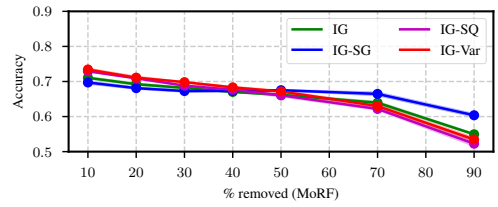
In Table 7, we show a full view of Spearman Correlation of rankings given by eight different evaluation strategies (“Retrain” / “No-Retrain”, MoRF/LeRF, and Noisy Linear/fixated imputation) used in this paper.



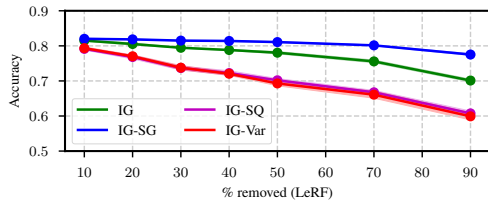
## Evaluating Feature Attribution: An Information-Theoretic Perspective



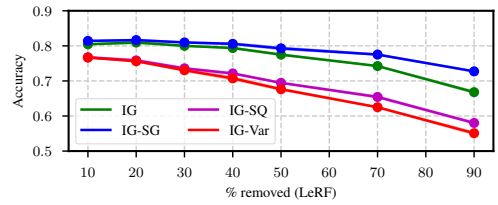
(a) MoRF: fixed imputation



(b) MoRF: Noisy Linear Imputation

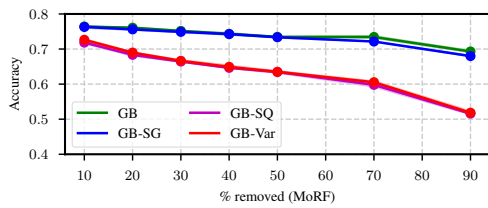


(c) LeRF: fixed imputation

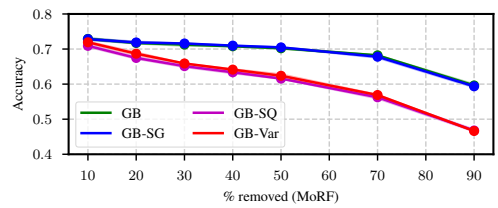


(d) LeRF: Noisy Linear Imputation

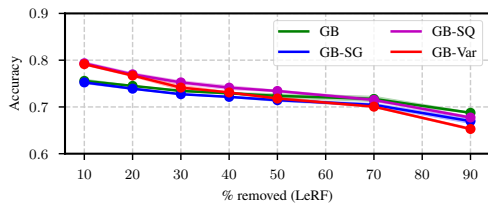
Figure 11. Consistency comparison using fixed value imputation vs. Noisy Linear Imputation of IG-based methods with retraining.



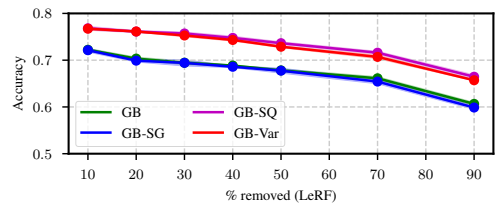
(a) MoRF: fixed imputation



(b) MoRF: Noisy Linear Imputation



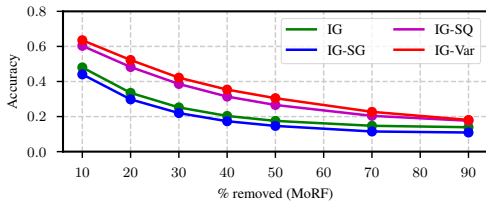
(c) LeRF: fixed imputation



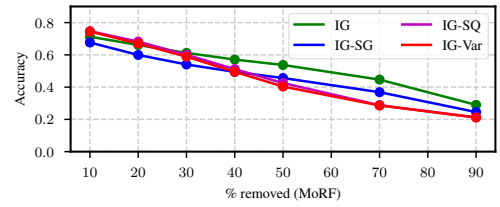
(d) LeRF: Noisy Linear Imputation

Figure 12. Consistency comparison using fixed value imputation vs. Noisy Linear Imputation of GB-based methods with retraining.

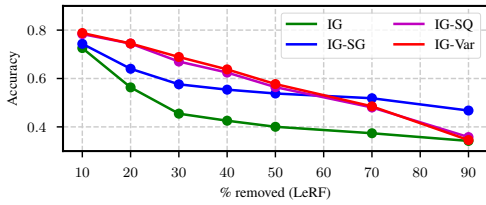
## Evaluating Feature Attribution: An Information-Theoretic Perspective



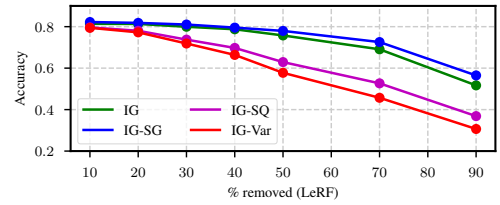
(a) MoRF: fixed imputation



(b) MoRF: Noisy Linear Imputation

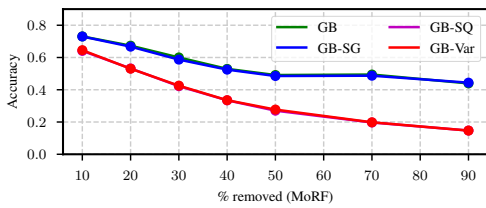


(c) LeRF: fixed imputation

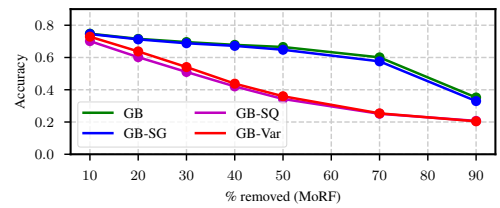


(d) LeRF: Noisy Linear Imputation

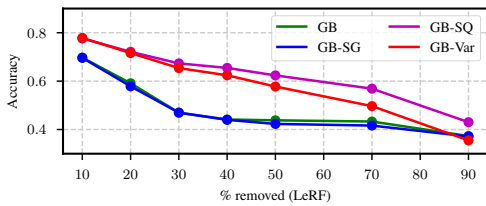
Figure 13. Consistency comparison using fixed value imputation vs. Noisy Linear Imputation of IG-based methods without retraining.



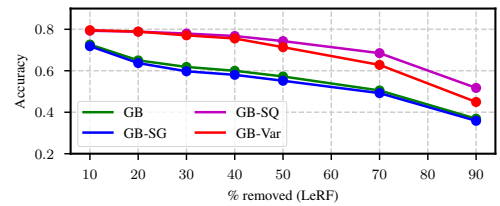
(a) MoRF: fixed imputation



(b) MoRF: Noisy Linear Imputation



(c) LeRF: fixed imputation



(d) LeRF: Noisy Linear Imputation

Figure 14. Consistency comparison using fixed value imputation vs. Noisy Linear Imputation of GB-based methods without retraining.